

Modeling of Persistent Homology

Sarit Agami and Robert J. Adler

Abstract. Topological Data Analysis (TDA) is a novel statistical technique, particularly powerful for the analysis of large and high dimensional data sets. Much of TDA is based on the tool of persistent homology, represented visually via persistence diagrams. In an earlier paper we proposed a parametric representation for the probability distributions of persistence diagrams, and based on it provided a method for their replication. Since the typical situation for big data is that only one persistence diagram is available, these replications allow for conventional statistical inference, which, by its very nature, requires some form of replication. In the current paper we continue this analysis, and further develop its practical statistical methodology, by investigating a wider class of examples than treated previously.

Keywords. Persistence diagram, Hamiltonian, MCMC, Replicated persistence diagrams.

1. Introduction and setting

The notion of persistent homology arises when one has a filtration of spaces; viz. a sequence (or continuum) of spaces $\mathcal{Z}_1 \subseteq \mathcal{Z}_2 \subseteq \dots$ (or \mathcal{Z}_t , with $\mathcal{Z}_s \subseteq \mathcal{Z}_t$ whenever $s \leq t$) and one is interested in how homology changes as one moves along the sequence. For a typical example, suppose that \mathcal{Z} is a nice space, and let $f : \mathcal{Z} \rightarrow \mathbb{R}$ be a smooth function. Denote by \mathcal{Z}_u the filtration of excursion, or upper-level, sets

$$\mathcal{Z}_u \triangleq \{z \in \mathcal{Z} : f(z) \in [u, \infty)\} \equiv f^{-1}([u, \infty)). \quad (1.1)$$

A useful way to describe persistent homology is via the notion of barcodes. Assuming that $\dim(\mathcal{Z}) = D$, the smoothness of f implies that, if \mathcal{Z}_u is non-empty, then $\dim(\mathcal{Z}_u)$ will typically also be D . A barcode for the excursion sets of f is then a collection of $D + 1$ diagrams, one for each collection of homology groups of common order. A bar in the k -th diagram, starting at u_1 and ending at u_2 ($u_1 \geq u_2$) indicates the existence of a generator of $H_k(\mathcal{Z}_u)$ that appeared at level u_1 and disappeared at level u_2 . A different, and visually helpful, representation of a bar is as a point (d, b) in the plane. Each bar has a ‘birth time’ b and ‘death time’ d , where $d < b$ since, as described above, the filtration is for upper level sets, and we index these by levels descending from $+\infty$. The collection of points (d, b) corresponding to all the bars is called the persistence diagram.

(We shall assume that the reader is familiar with these concepts. Recent excellent and quite different books and reviews by Carlsson [6, 7], Edelsbrunner and Harer [10, 11, 12], Zomorodian [17], Oudot [14] and Ghrist [13] not only give give broad expositions of homology, but also treat the much newer subject of persistent homology. (For a description of the history of persistent homology see the Introduction to [11].))

Persistence diagrams almost always arise as topological summaries of some underlying phenomenon, and, having been constructed, are typically subject to some kind of analysis. This can be thought of as a path

$$\textit{phenomenon} \rightarrow \textit{persistence diagram} \rightarrow \textit{analysis}. \quad (1.2)$$

The analysis can be of various forms. Wasserman [16] gives a comprehensive and up to date review on topological data analysis from the viewpoint of statistics, but there are also non-statistical approaches, many of which involve summarizing the diagram with either a low dimensional vector of numerical descriptors, a large dimensional vector, or a real valued function. Many of these approaches adopt techniques such as principal component analysis and support vector machines to analyse the summary data.

What is common to all these approaches, however, is the need for multiple instances of the persistence diagram, which in practical situations, is typically not a trivial requirement. Although, in some scenarios, multiple observations of the ‘phenomenon’ of (1.2) may be available, it is more common that only one observation of the phenomenon is available, and so only one diagram. In those cases, the standard method to effectively increase the number of instances is via resampling, either of the phenomenon or the diagram. Virtually all of the above approaches have examples of this method.

In a previous paper [2] we entered the diagram (1.2) at the intermediate step, by suggesting a new approach to providing multiple instances of a persistence diagram when, perhaps, only one such original diagram is available. This was done via probabilistic modeling of persistence diagrams. We shall briefly recall the basic ideas of [2] in Sections 2 and 3 below, and then develop them, in terms of more sophisticated examples than were treated there, in Section 4.

2. Parametric model

2.1. The basic setup

As above, let \mathcal{Z} be a compact subset of \mathbb{R}^D , typically a sub-manifold or stratified sub-manifold, and suppose that we observe a sample $\tilde{Z}_n = \{Z_1, \dots, Z_n\}$ drawn from a distribution P supported on \mathcal{Z} . Based on this sample, we define a kernel density estimator, \hat{f}_n , given by

$$\hat{f}_n(p) = \frac{1}{n(\sqrt{2\pi}\eta)^D} \sum_{i=1}^n e^{-\|p-z_i\|^2/2\eta^2}, \quad p \in \mathbb{R}^D, \quad (2.1)$$

where $\eta > 0$ is a bandwidth parameter for the Gaussian kernel defining \hat{f}_n .

Our interest is in the persistence diagram generated by the upper-level set filtration generated by \hat{f}_n ; viz. by the sets of (1.1) as u decreases from $+\infty$. The death and birth points in the diagram are denoted by $(d_i, b_i)_{i=1}^{N_k}$, where N_k is the number of points in the diagram for the homology of order k . Typically, we shall treat only one order at a time, and drop the subscript on N_k . Define a new set of N points $\tilde{x}_N = \{x_i\}_{i=1}^N$, with $x_i^{(1)} = d_i$ and $x_i^{(2)} = b_i - d_i$. That is, \tilde{x}_N is a set of N points in $\mathcal{X} = \mathbb{R} \times \mathbb{R}_+$. This (invertible) transformation has the effect of moving the points in the original persistence diagram downwards, so that the diagonal line projects onto the horizontal axis, but still leaves a visually informative diagram, called the projected persistence diagram, or PPD, in [2]. The first step towards the goal of a statistical analysis of the persistence diagram is to develop a parametric, probabilistic model for \tilde{x}_N .

2.2. The model

Following [2], as a first step of building a model for \tilde{x}_N , consider the Gibbs distribution,

$$\varphi_{\Theta}(\tilde{x}_N) = \frac{1}{Z_{\Theta}} \exp(-H_{\Theta}(\tilde{x}_N)), \quad (2.2)$$

where Θ is a multi-dimensional parameter, $H_\Theta : \mathcal{X} \rightarrow \mathbb{R}$ is a ‘Hamiltonian’ that describes the ‘energy’ of \tilde{x}_N , and Z_Θ is the normalizing ‘partition function’ required to make φ_Θ a probability density. The next step is to choose the Hamiltonian, which needs to take into account the spread of the N points, along with interactions between neighboring points, which we shall think of as belonging to clusters. Regarding the spread, define

$$\sigma_H^2 = \sum_{x \in \tilde{x}_N} (x^{(1)} - \bar{x}^{(1)})^2, \quad \sigma_V^2 = \sum_{x \in \tilde{x}_N} (x^{(2)})^2,$$

where $\bar{x}^{(1)} = N^{-1} \sum_{i=1}^N x_i^{(1)}$. Then σ_H^2 is the (un-normalized) variance of the horizontal points, and σ_V^2 is the L_2 power of the vertical points (not centered because of the non-negativeness of $x^{(2)}$). As for the local interaction, for $x \in \mathcal{X}$ and for $k \geq 1$ let $x^{nn}(k) \in \mathcal{X}$ be the k -th nearest neighbor of x , and set

$$\mathcal{L}_{\delta,k}(\tilde{x}_N) = \sum_{x \in \tilde{x}_N} \|x - x^{nn}(k)\| \mathbb{1}_{\{\|x - x^{nn}(k)\| \leq \delta\}}.$$

Then, as in [2], we choose the Hamiltonian

$$H_{\delta,\Theta}^K(\tilde{x}_N) = \theta_H \sigma_H^2 + \theta_V \sigma_V^2 + \sum_{k=1}^K \delta^{-2} \theta_k \mathcal{L}_{\delta,k}(\tilde{x}_N), \quad (2.3)$$

where $\Theta = (\theta_H, \theta_V, \theta_1, \dots, \theta_K)$, and K is the maximal cluster size. The inclusion of the normalising parameter δ^{-2} allows for the θ_k to be interpreted as energy densities, and improves the numerical stability of parameter estimation.

There are a number of reasons for this choice of Hamiltonian, among them:

- (i) Cluster expansions of this form have been successfully employed in Statistical Mechanics for the best part of a century as a basic approximation tool in the study of particle systems. More specifically, for the model to be rich enough for TDA, one needs to choose the Hamiltonian from a parameterised family that comes close to spanning all ‘reasonable’ functions on PPDs. Since [1] showed that the ring of algebraic functions on the space of PPDs is spanned by a family of monomials closely related to functions of the form (2.3), this choice of Hamiltonian is an effective one for our setting.
- (ii) These distributions are often used not as exact models for PPDs, but rather as a tool in a perturbative analysis. In these cases, the convenience of the models is more important than whether or not they provide a perfect fit to PPD data. For more details see [2], SI (Sec. 2.2).

Finally, δ is determined by

$$\delta = \frac{\delta^*}{N^{\alpha_{k,d}}} \max \left(\max |x_i^{(1)} - x_j^{(1)}|, \max |x_i^{(2)} - x_j^{(2)}| \right), \quad (2.4)$$

where $\alpha_{0,d} = 1/d$, $\alpha_{k,d} = k/(k+1)d$, for $k \geq 1$, d is the dimension of the data underlying the persistence diagram, and δ^* is a data independent tuning parameter. Although we typically optimize over δ^* , it can be taken to be $N^{-1/2}$, as a global default.

2.3. Estimation and model specification

Since there is no analytic form for Z_Θ and it is impossible to compute it numerically in any reasonable time, we cannot estimate Θ by maximum likelihood. A standard way around this, adopted in [2], is to use pseudolikelihood estimation [3, 8]; viz. to maximize the pseudolikelihood

$$L_{\delta,\Theta}^K(\tilde{x}_N) \triangleq \prod_{x \in \tilde{x}_N} f_\Theta(x | \mathcal{N}_{\delta,K}(x)). \quad (2.5)$$

Here $\mathcal{N}_{\delta,K}(x)$ denotes the collection of the K nearest neighbours of x in \tilde{x}_N whose distance from x is no greater than δ , and

$$f_{\Theta}(x|\mathcal{N}_{\delta,K}(x)) = \frac{\exp\left(-H_{\delta,\Theta}^K(x|\mathcal{N}_{\delta,K}(x))\right)}{\int_{\mathbb{R}} \int_{\mathbb{R}_+} \exp\left(-H_{\delta,\Theta}^K(z|\mathcal{N}_{\delta,K}(x))\right) dz^{(1)} dz^{(2)}, \quad (2.6)$$

with

$$H_{\delta,\Theta}^K(x|\mathcal{N}_{\delta,K}(x)) = \theta_H \left[x^{(1)} - \bar{x}^{(1)} \right]^2 + \theta_V (x^{(2)})^2 + \sum_{k=1}^K \delta^{-2} \theta_k \mathcal{L}_{\delta,k}(\mathcal{N}_{\delta,K}(x)).$$

Optimal values of K can be chosen via standard, automated, statistical procedures such as AIC, BIC, etc (cf. [5]). However, considerable experimentation, much of it reported in [2], leads to the conclusion that it suffices to take $K = 2$ or $K = 3$, so that the largest cluster size is 3 or 4.

3. Replicating persistence diagrams

3.1. MCMC

Once the parametric distribution of the points of the persistence diagram is available, as in the pseudolikelihood (2.5), simulated replications of the diagram can be generated using a standard Metropolis-Hastings MCMC algorithm [15, 4]. Firstly, given a \tilde{x}_N , define a ‘proposal distribution’ $q(\cdot|\tilde{x}_N)$ as the bivariate Gaussian density, with mean vector and covariance matrix identical to the empirical mean and covariance of the points in \tilde{x}_N , but restricted to $\mathbb{R} \times \mathbb{R}_+$. Next, for two points $x, x^* \in \mathbb{R} \times \mathbb{R}_+$ define an ‘acceptance probability’, according to which $x \in \tilde{x}_N$ is replaced by x^* , leading to the updated PPD \tilde{x}_N^* , as

$$\rho(x, x^*) = \min \left\{ 1, \frac{f_{\Theta}(x^*|\mathcal{N}_{\delta,K}(x)) \cdot q(x|\tilde{x}_N^*)}{f_{\Theta}(x|\mathcal{N}_{\delta,K}(x)) \cdot q(x^*|\tilde{x}_N)} \right\}.$$

Then the algorithm is Algorithm 1.

Algorithm 1 MCMC step updating diagram for \tilde{x}_N

- 1: $k = 0$
 - 2: $k \leftarrow k + 1$
 - 3: Choose x^* according to $q(\cdot|\tilde{x}_N)$
 - 4: Compute $\rho(x_k, x^*)$
 - 5: Choose U a standard uniform variable on $[0, 1]$
 - 6: **if** $U < \rho(x_k, x^*)$ **then** set $x_k = x^*$
 - 7: **end if**
 - 8: **if** $k < N$ **then** go to Step 2
 - 9: **end if**
-

To obtain M approximately independent PPD’s, [2] adopt a procedure dependent on three parameters, n_b , n_r and n_R , as follows. Starting with the original PPD, run the algorithm for a burn in period. Then, starting with the final PPD from the burn in, run the algorithm a further n_b times, choosing the last output of this block of n_b iterations as the first simulated PPD. Repeat this procedure n_r times, each time starting with the most recently simulated PPD; viz. the output of the previous block. Finally, replicate the entire procedure n_R times, for a total of $n = n_r \times n_R$ simulated PPDs. The optimal choice of n_b , n_r and n_R typically depends on the specific problem, and is discussed in [2] SI (Sec. 2.1). The burn in period is determined, empirically, via the evaluation of the

distance between the MCMC simulations and the original persistence diagrams. Recall that, for two diagrams D_1 and D_2 , the Wasserstein p -distance, $W_p(D_1, D_2)$, $p > 0$, is defined as

$$W_p(D_1, D_2) = \inf_{\gamma} \left(\sum_{u \in D_1} \|u - \gamma(u)\|_{\infty}^p \right)^{1/p} \quad (3.1)$$

where γ ranges over all matchings between the points of D_1 and D_2 , the latter having been augmented by adding all points on the diagonal. In the limit case of $p = \infty$ the Wasserstein distance is known as the bottleneck distance, which is the length of the longest edge in the best matching.

The distances between the MCMC simulations and the original persistence diagrams are measured via the bottleneck and Wasserstein distances as the MCMC progresses, and the value of the burn in period is chosen as the point at which the initial rapid growth of the distance functions ceases. Given the collection of M simulated PPDs, each PPD is converted back to a regular persistence diagram with the mapping $x \rightarrow (x^{(1)}, x^{(1)} + x^{(2)}) = (d, b)$ of its component points.

3.2. Identification of topological signals

In many situations, which include all the examples that we shall treat in this paper, the most prominent features of the persistence diagram are generally deemed most likely to represent true features of the underlying space, rather than artifacts of sampling or noise. By ‘prominent’ we mean those points in the diagrams which are furthest from the diagonal. These are typically called ‘topological signals’, while the points closer to the diagonal are considered to be ‘topological noise’.

One of the key challenges in persistent homology is to separate the signal from the noise. The replicated persistence diagrams can be used to identify the topological signals by providing information about statistical variation. As an example, consider the order statistics of the distances of the points of the persistence diagram to the diagonal. That is, given the points (d_i, b_i) of the persistence diagram, the order statistics are T_j , the j -th largest among the differences $|b_i - d_i|$, $j = 1, \dots, N$.

Denote by \hat{T} the value of the relevant statistic based on the true persistence diagram, and denote by \hat{T}^* the value of the relevant statistic based on the simulated persistence diagram. Then one can calculate an empirical confidence interval (percentile bootstrap) $[c_1, c_2]$ and define a point on the persistence diagram to be a signal if $\hat{T} < \hat{c}_1$ or $\hat{T} > \hat{c}_2$. Note that since here T is non-negative, we generally only consider one-sided confidence intervals $[0, \hat{T} + \hat{c}_2]$. In addition, one can calculate a one-side p -value as $\frac{1}{M} \sum_{m=1}^M \mathbb{1}(\hat{T}_m^* \geq \hat{T})$, where \hat{T}_m^* is \hat{T}^* of the m -th simulated persistence diagram.

4. Examples

We now turn to the three examples which make up the new material of this paper. In each of these we show how to use the methodology described in the previous sections to identify the homology of spaces \mathcal{Z} , when all that is available is the persistence diagram generated by the upper level sets of a smoothed empirical density from a sample. The examples that we shall treat are those of a 2-sphere, a 2-torus and a collection of three concentric circles in the plane. Each of these will teach us something different about the behaviour of our methodology in practice.

4.1. The two dimensional sphere

4.1.1. The data and fitting the model. We start with a random sample of $n = 1,000$ points from the uniform distribution on the sphere S^2 in R^3 with radius $r = 1$, and smooth the data with a kernel density estimator of bandwidth of $\eta = 0.1$. These are shown as Panels (a) and (b) of Figure 1.

The corresponding persistence diagram of the upper level sets filtration of \hat{f}_N is shown in Panel (c) of Figure 1. This diagram contains $N_0 = 110$ points corresponding to the zeroth homology H_0 , represented by the black circles, $N_1 = 74$ points for the first homology H_1 , represented by the red triangles, and $N_2 = 1$ point for the second homology H_2 , represented by the blue diamond.

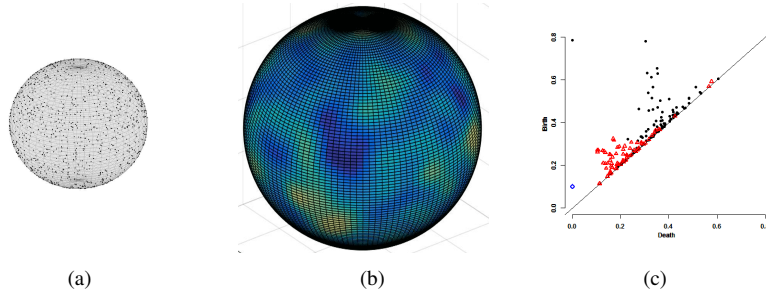


FIGURE 1. (a) Points sampled from a unit sphere. (b) The corresponding kernel density estimator, shown, for visual clarity, at only a few quantized levels. (c) The corresponding persistence diagram for the upper level sets of the kernel density estimate on the full sphere. Black circles are H_0 persistence points, red triangles are H_1 points, and the blue diamond is the H_2 persistence point. Birth times are on the vertical axis.

As described above, each point in the diagram is a ‘death-birth’ pair (d, b) . Since we know that the upper level sets of \hat{f}_N are characterized by having a single connected component and a single void, we expect to have one black circle somewhat isolated from the other points in the diagram and one blue diamond. The void does not have to be isolated from the other points due to a short lifetime of high dimensional homologies. This is in fact the case.

While the persistence diagram in Figure 1 performs as expected, and it is easy to identify the points that, a priori, we knew had to be there, there are many other points in the diagram which, were we not in the situation of knowing ahead of time, and we would have difficulty in knowing how to discount.

Note that there are more than enough H_0 and H_1 points in Figure 1 to fit a spatial model to each of the two homologies.

Adopting the approach described in the first three sections of the paper, and working first with the H_0 persistence diagram without including the ‘point at infinity’¹, we estimated the parameters for a Gibbs distribution for the model with pseudolikelihood (2.5), taking $K = 3$. The estimate of δ was 0.0051. For this δ , the estimates of Θ were $\theta_1 = -0.0339$, $\theta_2 = -0.0210$, $\theta_3 = -0.0120$, $\theta_H = 72.80$, and $\theta_V = 39.50$.

In order to test how well the estimated model matches the persistence diagram, we followed the procedure described in [2]. We generated 100 collections of samples from the 2-sphere according the same procedure that generated the original data, and for each we fitted the model we found for the original data set; viz. the model that includes the parameters $\theta_1, \theta_2, \theta_3, \theta_H$, and θ_V .

The blue plot in Figure 2 shows the (smoothed) empirical densities of the resulting parameter estimates². (We will discuss the other two plots only later, when considering different replication procedures.) Overall, the results indicate that the estimation procedure is stable, with an acceptable spread.

¹In all our persistence diagrams, the ‘point at infinity’ is the highest, leftmost point in the H_0 diagram. In essence, removing it from the analysis is much like working with reduced rather than standard homology, and has the effect of removing one generator from the H_0 diagram. Thus, in the statistical analysis to follow, it needs to be added, at the end, to all significant points found in the diagram.

²In some of these simulations the sums $L_{\delta,k}$ were identically zero for all $k = 1, 2, 3$ simultaneously, since there were no k -th nearest neighbours at distance less than δ . Consequently, the parameters θ_1, θ_2 , and θ_3 are all meaningless, and so these simulations (33 of them) were deleted from this part of the analysis. We shall do the same later on, in similar cases, without further comment.

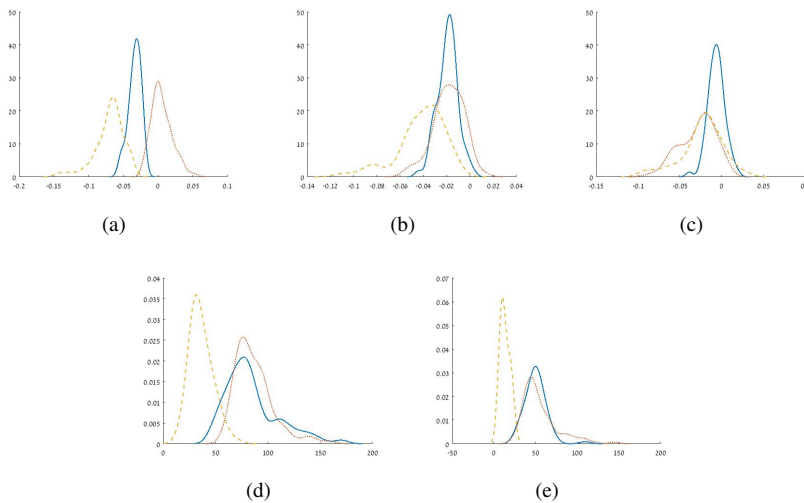


FIGURE 2. Smoothed empirical densities for the five parameter estimates in the Hamiltonian (2.3) for the H_0 persistence diagram coming from the simulations of 2-sphere and from resampling, see text for details. (a) θ_1 , (b) θ_2 , (c) θ_3 , (d) θ_H , (e) θ_V .

4.1.2. Replicating the persistence diagram. For the calculation of the replicated persistence diagrams, we first need to determine the burn in period which we shall use for them. Following the procedure described in Section 3.1 we calculated the bottleneck and Wasserstein distances using the 100 simulated persistence diagrams of the previous subsection. The results are shown in blue in Figure 3.

The first row in Figure 3 shows the bottleneck distances, while the second row shows the W_2 differences. The first column shows the results of the first 50 steps of the MCMC algorithm on a linear scale. The second and third columns go out to 2,000 steps, first on a linear scale and then on a logarithmic scale. While the initial growth of the distances is rapid, they eventually approach their asymptotes at exponential rates. The rapidity is clear in Panels (a) and (d), and the exponential rate is clear from the linear behavior of the plot in logarithmic scales. The point where the initial rapid growth of the distance functions ceases is approximately 44 for the bottleneck distance and 47 in the Wasserstein case. At 44 steps, therefore, the results of Figure 3 indicate that the dependence of the MCMC on the initial persistence diagram has dropped significantly, while at the same time the MCMC has produced persistence diagrams remaining close to the true distribution.

In addition we considered summary statistics of the 100 persistence diagrams as the MCMC progressed, to see how well the simulations replicate the statistical properties of the persistence diagrams. The results are presented in Figure 4. Overall, the best fits are at burn in of 10, 25 and 50, which is consistent with the results of Figure 3.

4.1.3. Resampling. The replicated persistence diagrams described in the previous subsection were based on knowing, a priori, that the original data was generated by sampling from a 2-sphere. The typical real-life situation is that one does not know the space generating the persistence diagram. (If one did, it would hardly be necessary to estimate its homology by sampling.) Consequently, we now look at resampling as a method for generating replications of the persistence diagram.

There are two natural approaches based on resampling. One is to resample from the original persistence diagram (“Setting I”), and another is to resample from the original data (“Setting II”). We examined both these alternatives, repeating them 100 times.

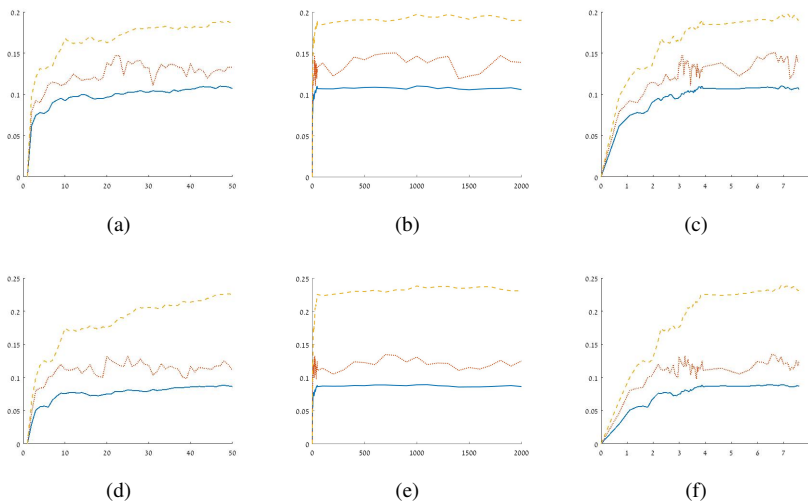


FIGURE 3. Growth of the bottleneck (a) and Wasserstein (d) differences of MCMC simulations from a specific persistence diagram (vertical axis), as a function of the number of steps n_b (horizontal axis, $1 \leq n_b \leq 50$) averaged over 100 independent persistence diagrams. Panels (b) and (e) take $1 \leq n_b \leq 2,000$, while (c) and (f) show the same data but on a logarithmic scale.

The results of these approaches are the other two plots of Figure 2. The red (dot dashed) plot is the smoothed empirical density for the parameter estimates based on resampled sets from the original persistence diagram, and the yellow (dashed) plot corresponds to the resampled sets from the original data.

In order to assess the fit of the simulated data to the original, we computed, as previously, the bottleneck and the Wasserstein distances between the MCMC simulations and the data itself. The results are in Figure 3, in addition to the results based on the 100 simulated persistence diagrams. The red (dot dashed) plot shows the results for the 100 resampled sets from the original persistence diagram, and the yellow (dashed) plot corresponds to the 100 resampled sets from the original data. The point where the initial rapid growth of the distance functions ceases is approximately 22 and 46, respectively, in Setting I and Setting II for the bottleneck distance, and approximately 20 and 48 in the Wasserstein case. This suggests taking a burn in period of 50 for generating the replicated persistence diagrams for H_0 .

4.1.4. H_1 persistence diagram. We now turn to the analysis of the H_1 persistence diagram. Again estimating the parameters for the Gibbs pseudolikelihood (2.5), taking $K = 3$, the estimate of δ was 0.0047. For this δ , the estimates of Θ were $\theta_1 = -0.0331$, $\theta_2 = 0$, $\theta_3 = 3.3842$, $\theta_H = 60.00$, and $\theta_V = 110.00$.

To check the match between the estimated model and the H_1 persistence diagram, we used the same 100 simulated sets of the 2-sphere used for the H_0 diagram, following the same procedure that we adopted then, this time restricting to a model with only θ_1 , θ_3 , θ_H , and θ_V non-zero. The blue plot in Figure 5 shows the smoothed empirical densities for the parameter estimates generated by these simulations. As for the H_0 case, the results indicate that the estimation procedure is stable.

4.1.5. Replicating the H_1 persistence diagram. As for the analysis of the H_0 diagram, we calculated bottleneck and the Wasserstein distances between the original persistence diagram using those

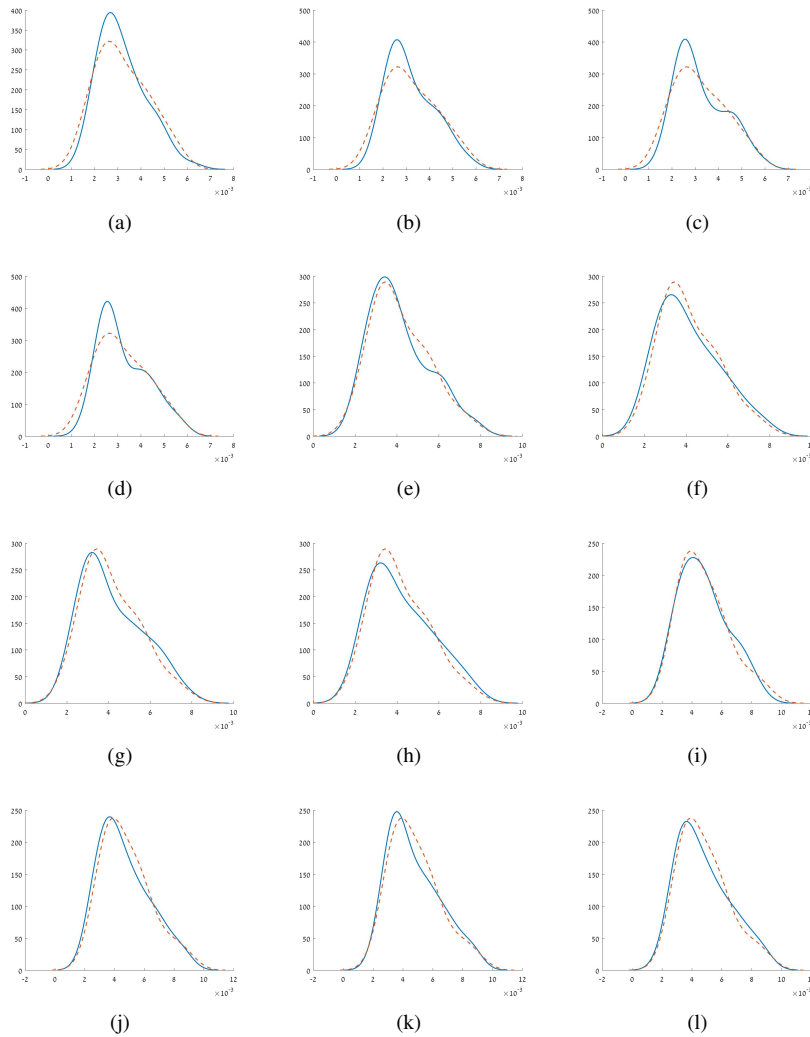


FIGURE 4. Summary statistics of average interaction strengths for 100 persistence diagrams. From left to right: cluster sizes 2, 3, and 4. From top to bottom, after 10, 25, 50, and 1,000 MCMC steps. See text for details.

corresponding to 100 MCMC simulated diagrams of the previous section. The results are shown by the blue plots in Figure 6.

The first row in Figure 6 shows the bottleneck distances, while the second row shows the W_2 differences. The first column shows the results of the first 50 steps of the MCMC algorithm on a linear scale. The second and third columns go out to 2,000 steps, first on a linear scale and then on a logarithmic scale. The point where the initial rapid growth of the distance functions ceases, is approximately 44 for the bottleneck distance and 47 in the Wasserstein case.

In addition we considered summary statistics of the 100 simulated persistence diagrams as the MCMC progressed, to ensure that the simulations reliably replicate the statistical properties of the persistence diagrams. Here the best fits were for a burn in of 50, which is consistent with the results of Figure 6.

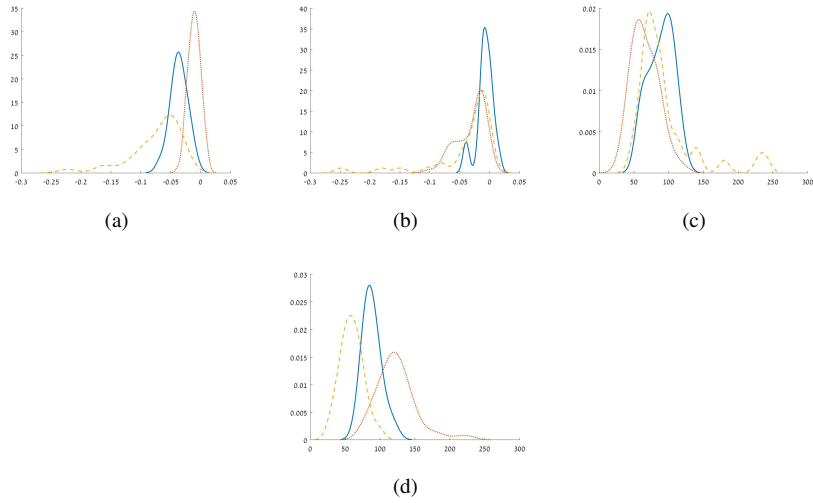


FIGURE 5. Smoothed empirical densities for the four parameter estimates of H_1 persistence diagram coming from the simulations of 2-sphere, see text for details. (a) θ_1 , (b) θ_3 , (c) θ_H , (d) θ_V .

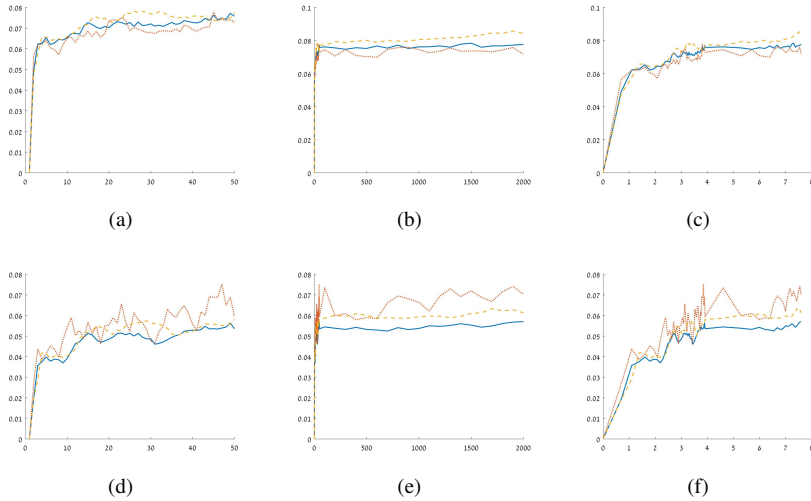


FIGURE 6. Growth of the bottleneck (a) and Wasserstein (d) differences of MCMC simulations from a specific persistence diagram (vertical axis), as a function of the number of steps n_b (horizontal axis, $1 \leq n_b \leq 50$) averaged over 100 independent persistence diagrams. Panels (b) and (e) take $1 \leq n_b \leq 2,000$, while (c) and (f) show the same data but on a logarithmic scale.

4.1.6. Resampling H_1 . As for the H_0 case, we again examine the performance of resampling from the original persistence diagram (Setting I) and from the original data (Setting II), repeating each procedure 100 times. The results are summarised in Figure 5. The red (dot dashed) plots are the smoothed empirical densities for the parameter estimates in Setting I, while the yellow (dashed) plot correspond to Setting II.

In order to assess the fit of the simulated data to the original, we computed, as previously, the bottleneck and the Wasserstein distances between the MCMC simulations and the data itself. The results are presented in Figure 6, in addition to the results based on the 100 simulated persistence diagrams. The red (dot dashed) plot shows the results for the 100 resampled sets from the original persistence diagram, and the yellow (dashed) plot shows the same thing, but for the 100 resampled sets from the original data. The point where the initial rapid growth of the distance functions ceases, is approximately 22 and 46 in Setting I and Setting II, respectively, for the bottleneck distance, and approximately 20 and 48 in the Wasserstein case. This suggests taking a burn in period of 50 for generating the replicated persistence diagrams for H_1 .

4.1.7. Statistical inference. We are now finally in a position to carry out a simulation study to test how well we can identify the homology of 2-sphere, using the methodology described earlier. To do so, we generated 1,000 persistence diagrams from the fitted model, via MCMC, with a burn in period of 50 iterations and with (n_b, n_r, n_R) given by (500,10,100), (500,20,50), (500,40,25), or (500,100,10). Using these four sets of simulations, we computed the maximum statistics T_1 , its confidence interval and its p -value, for both the H_0 and H_1 persistence diagrams. Table 1 summarizes the results.

homology	statistic	real PD	(n_b, n_r, n_R)	CI	p -value	significance
H_0	T_1	0.4769	(500,10,100)	[0, 0.4769]	0.0990	no
			(500,20,50)	[0, 0.4769]	0.0520	no
			(500,40,25)	[0, 0.3273]	0.0320	yes
			(500,100,10)	[0, 0.2616]	0.0100	yes
H_1	T_1	0.1673	(500,10,100)	[0, 0.2140]	0.4060	no
			(500,20,50)	[0, 0.2069]	0.3780	no
			(500,40,25)	[0, 0.2065]	0.3550	no
			(500,100,10)	[0, 0.1995]	0.3270	no

TABLE 1. Maximum statistic T_1 for the real H_0 and H_1 persistence diagram and the simulated H_0 and H_1 persistence diagrams of the 2-sphere. The CI is a one-sided confidence interval at a 5% confidence level. The p -value is also one-sided. Both the CI and the p -value are based on 1,000 simulated persistence diagrams.

The results for the H_0 persistence diagram show that T_1 , in two first scenarios, was statistically insignificant, and in the two other scenarios was significant. In other words, the evidence is split between one connected component (represented by the ‘point at infinity’ not included in the analysis) and two components. The fact that the correct result occurs in the cases of a larger number of shorter MCMC runs is consistent with earlier findings in [2].

As for the H_1 topology, all four scenarios showed that T_1 was insignificant for all MCMC parameter, implying, correctly, a trivial H_1 homology.

4.2. 2-torus

We now turn to our second example, that of the two-dimensional torus. Since the analysis will be similar in approach to that for the two-dimensional sphere, we will give fewer details, concentrating primarily on the more important differences in the results.

4.2.1. The data and fitting the model. This example includes a sample of $n = 1,000$ points from the 2-torus $T^2 = S^1 \times S^1$ in R^3 , chosen uniformly with respect to the natural Riemannian metric induced on it as a subset on \mathbb{R}^3 . This leads to the high density of points in the ‘interior’ of the torus, obvious from Figure 7. (For more details on sampling from tori and other manifolds, see [9].) More specifically, the torus was taken to be the rotation about the ‘ z axis’ in \mathbb{R}^3 of a circle of radius 1.8 with center in the ‘ (x, y) plane’ at distance 2 from the origin.

Panel (a) in Figure 7 shows the sample superimposed on the torus, and Panel (b) shows the corresponding kernel density estimator based on a bandwidth of $\eta = 0.2$. The corresponding persistence diagram of the upper level set filtration of \hat{f}_N is Panel (c). This diagram contains $N_0 = 216$ points of the zeroth homology H_0 , represented by the black circles, $N_1 = 160$ points of the first homology H_1 , represented by the red triangles, and $N_2 = 216$ points of the second homology H_2 , represented by the blue diamonds. Since we know that the upper level sets of \hat{f}_N are characterized by having a single connected component, two holes, and a single void, we expect to have one black circle and two red triangles somewhat isolated from the other points in the diagram, and one blue diamond. In fact, we can see the one isolated black circle point, but it is not clear which are the two main red triangles.

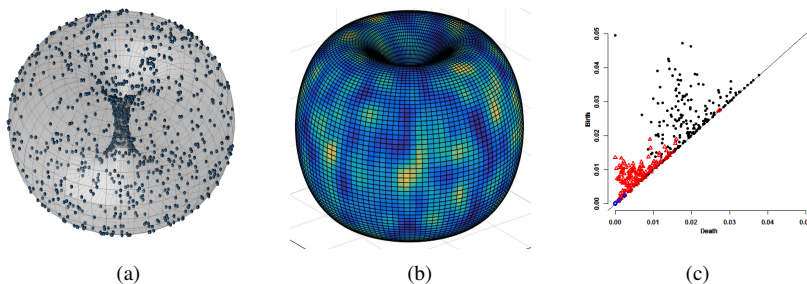


FIGURE 7. (a) Points sampled from a torus. View from above the torus. (b) The corresponding kernel density estimator, shown, for visual clarity, at only a few quantized levels, and from a different angle to (a). (c) The corresponding persistence diagram for the upper level sets of the kernel density estimate on the full torus. Black circles are H_0 persistence points, red triangles are H_1 points, blue diamonds are H_2 persistence points. Birth times are on the vertical axis.

Adopting the approach described above separately for the H_0 and H_1 persistence diagrams, we estimated the parameters for a Gibbs distribution for the model with pseudolikelihood (2.5), taking $K = 3$. For the H_0 diagram, working without the point at infinity, the estimate of δ was 0.0010, and the estimates of Θ were $\theta_1 = -0.0034$, $\theta_2 = -0.0026$, $\theta_3 = -0.0032$, $\theta_H = 1.08E + 04$, and $\theta_V = 4.19E + 03$.

For the H_1 persistence diagram, the estimate of δ was 0.0007, and the estimates of Θ were $\theta_1 = -0.0044$, $\theta_2 = -0.0059$, $\theta_3 = -0.0036$, $\theta_H = 1.29E + 05$, and $\theta_V = 1.50E + 04$.

4.2.2. Replicating the persistence diagram. The determination of the burn in period in this example, for both H_0 and H_1 , was only heuristic. Figure 8 presents the original persistence diagrams of H_0 and H_1 and their MCMC with burn in periods of 10, 25, 50 and 1000. The best fits for both H_0 and H_1 occur for burn in periods in the range $[10, 50]$.

4.2.3. Statistical inference. We generated 1,000 replicated persistence diagrams from the fitted model with a burn in period of 10 iterations and with (n_b, n_r, n_R) given by (500,10,100), (500,20,50), (500,40,25), or (500,100,10). Using these four sets of simulations, we computed the maximum statistics T_j , $j = 1, \dots, 4$, their confidence intervals and their p -values. Table 2 summarizes the results.

The results for the H_0 diagram, for all scenarios, showed that T_1 was insignificant (the lowest p -value reached in any of the six cases was 0.235). Thus, adding the ‘point at infinity’ back into the diagram, we have evidence for exactly one connected component, as we hoped to find.

For the H_1 diagram, the results for all scenarios showed that T_1 and T_2 were significant (the highest p -value reached in any of the 8 cases was 0.049). That is, two significant holes, as we hoped to find.

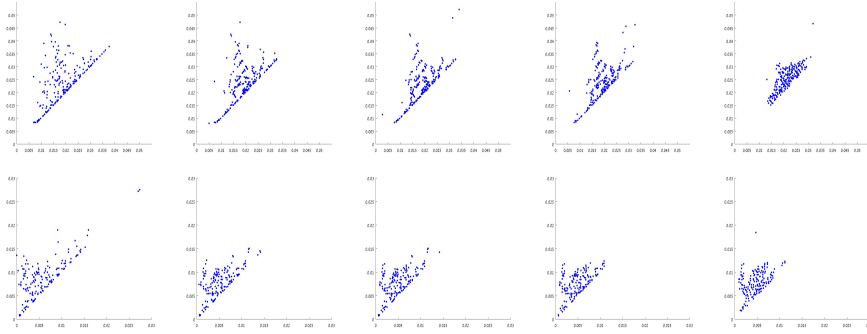


FIGURE 8. The first row shows the persistence diagrams of H_0 , and the second row shows the persistence diagrams of H_1 . At each row, the left plot is the original persistence diagram, and the four other plots are simulated persistence diagrams based on an MCMC simulation with burn in of 10, 25, 50 and 1000.

homology	statistics	real PD	(n_b, n_r, n_R)	CI	p -value	significance
H_0	T_1	0.0295	$(500,10,100)$	$[0, 0.0371]$	0.3360	no
			$(500,20,50)$	$[0, 0.0362]$	0.2770	no
			$(500,40,25)$	$[0, 0.0359]$	0.2350	no
			$(500,100,10)$	$[0, 0.0322]$	0.2720	no
H_1	T_1	0.0136	$(500,10,100)$	$[0, 0.0123]$	0.0340	yes
			$(500,20,50)$	$[0, 0.0118]$	0.0320	yes
			$(500,40,25)$	$[0, 0.0107]$	0.0220	yes
			$(500,100,10)$	$[0, 0.0134]$	0.0490	yes
H_1	T_2	0.0118	$(500,10,100)$	$[0, 0.0103]$	0.0030	yes
			$(500,20,50)$	$[0, 0.0102]$	0.0060	yes
			$(500,40,25)$	$[0, 0.0102]$	0	yes
			$(500,100,10)$	$[0, 0.0101]$	0.0020	yes
H_1	T_3	0.0103	$(500,10,100)$	$[0, 0.0100]$	0.0360	yes
			$(500,20,50)$	$[0, 0.0098]$	0.0060	yes
			$(500,40,25)$	$[0, 0.0099]$	0.0060	yes
			$(500,100,10)$	$[0, 0.0099]$	0.0180	yes

TABLE 2. Maximum statistics T_1, T_2, T_3 for the real H_0 and H_1 persistence diagrams and the simulated H_0 and H_1 persistence diagrams of the 2-torus. The CI is a one-sided confidence interval at a 5% confidence level. The p -value is also a one-sided. Both the CI and the p -value are based on 1000 simulated persistence diagrams.

Unfortunately, however, T_3, \dots, T_8 were also statistically significant, leading to a significantly over-estimation of the complexity of the H_1 homology. This seems to be due to the sparsity of points in the sample, which is clear from the first two panels in Figure 7. Our conclusion here, therefore, is a need for either a larger sample size or, perhaps, a larger bandwidth for the kernel density estimator.

4.3. Three circles

Our final example is that of three concentric circles in \mathbb{R}^2 . We describe the main results, skimming on detail.

4.3.1. The data and fitting the model. For this example we start with a random sample of $n = 1,200$ points from three circles, of diameters 6, 4 and 1, as shown in the Panel (a) of Figure 9. In total, 600 points were chosen from the largest circle, 400 from the middle circle, and 200 from the smallest one. Panel (b) shows the corresponding kernel density estimate, for which we took the bandwidth $\eta = 0.1$. Panel (c) displays the corresponding persistence diagram of the upper level set

filtration of \hat{f}_N , containing $N_0 = 80$ points of the zeroth homology H_0 , represented by the black circles, with the red triangles corresponding to the first homology H_1 . Since we know that the upper level sets of \hat{f}_N are characterized by having three main components, each of which contains a single 1-cycle (hole) we expect to see three black circles and three red triangles somewhat isolated from the other points in the diagram, which is in fact the case.

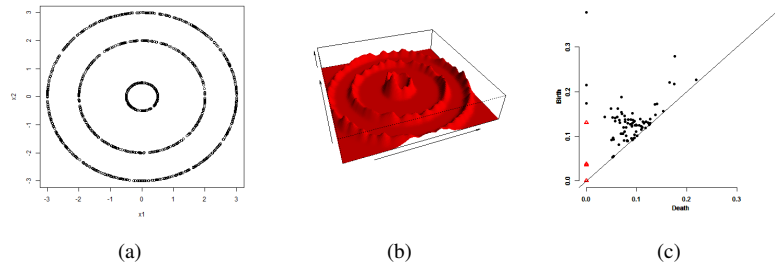


FIGURE 9. (a) A random sample from three circles, 600 points from the larger circle, 400 points from the middle circle, and 200 from the smaller one, with a kernel density estimate (b) and the persistence diagram (c) for its upper level sets. Black circles are H_0 persistence points, red triangles are H_1 points. Birth times are on the vertical axis.

Note firstly that while there are quite a few (black, circular) points corresponding to the H_0 homology, there are only four (red, triangular) for H_1 . Since the methodology described in the previous sections requires the estimation of a sophisticated model with a number of parameters, it follows that it is not appropriate for modelling the H_1 part of the diagram. However, there are more than enough H_0 points in Figure 9 to fit a spatial model to them.

Adopting the approach described above, and working only with the H_0 persistence diagram without including the ‘point at infinity’, we estimated the parameters for a Gibbs distribution for the model with pseudolikelihood (2.5), taking $K = 3$. The estimate of δ was 0.0012. For this δ , the estimates of Θ were $\theta_1 = -0.0105$, $\theta_2 = 0$, $\theta_3 = 0$, $\theta_H = 394.6$, and $\theta_V = 147.7$.

4.3.2. Statistical inference. We computed, as previously, the bottleneck and the Wasserstein distances between the MCMC simulations and the data itself, based on 100 simulated sets that behave the same as our original data. The point where the initial rapid growth of the distance functions ceases was approximately 10 for the bottleneck distance and was approximately 15 in the Wasserstein case. Based on these results, we generated 1,000 persistence diagrams from the fitted model with a burn in period of 10 iterations and with (n_b, n_r, n_R) given by (500,20,50), (500,40,25), or (500,100,10). Using these three sets of simulations, we computed the maximum statistics T_j , $j = 1, 2, 3$, their confidence intervals and their p -value. Table 3 summarizes the results.

The results, for all three scenarios, showed that T_1 and T_2 were highly significant (the largest p -value reached in any of the six cases was 0.003). In none of the three scenarios was T_3 significant, with p -values in the range (0.099, 0.117). That is, we found that the two points in the H_0 persistence diagram (as well as the ‘point at infinity’, which, recall, we removed from the analysis) are significant. Therefore we have three connected components, as we hoped to find.

References

- [1] Adcock, Aaron and Carlsson, Erik and Carlsson, Gunnar. *The ring of algebraic functions on persistence bar codes*. Homology, Homotopy and Applications **18** (2016), 381–402.

statistics	real PD	(n_b, n_r, n_R)	CI	p -value	significance
T_1	0.2145	(500,20,50)	[0, 0.1848]	0.0010	yes
		(500,40,25)	[0, 0.1750]	0.0020	yes
		(500,100,10)	[0, 0.1713]	0	yes
T_2	0.1740	(500,20,50)	[0, 0.1428]	0.0030	yes
		(500,40,25)	[0, 0.1402]	0.0010	yes
		(500,100,10)	[0, 0.1424]	0.0020	yes
T_3	0.1180	(500,20,50)	[0, 0.1250]	0.1150	no
		(500,40,25)	[0, 0.1232]	0.0990	no
		(500,100,10)	[0, 0.1244]	0.1170	no

TABLE 3. Maximum statistics T_1 , T_2 and T_3 for the real persistence diagram and the simulated persistence diagrams of the three circles. The CI is a one-sided confidence interval at a 5% confidence level. The p -value is also one-sided. Both the CI and the p -value are based on 1,000 simulated persistence diagrams.

- [2] Adler, R. J. and Agami, S. and Pranav, P. *Modeling and replicating statistical topology, and evidence for CMB non-homogeneity*. Proc. Nat. Acad. Sci., Web version, October 2017, doi: 10.1073/pnas.1706885114.
- [3] Besag, Julian. *Spatial interaction and the statistical analysis of lattice systems*. Journal of the Royal Statistical Society. Series B. Methodological **36** (1974), 192–236.
- [4] Brooks, S. and Gemna, A. and Jones, G.L. and Meng, X-L. *Handbook of Markov Chain Monte Carlo*. Chapman and Hall, Boca Raton (2011).
- [5] Burnham, Kenneth P. and Anderson, David R. *Model Selection and Multimodel Inference*. Springer-Verlag, New York (2002).
- [6] Carlsson, G., *Topology and data*, Bull. Amer. Math. Soc. (N.S.), **46**, 255–308, (2009).
- [7] Carlsson, G., *Topological pattern recognition for point cloud data*, Acta Numer., **23**, 289–368, (2014).
- [8] Chalmond, B. *Applied Mathematical Sciences*. Springer-Verlag, New York (2003).
- [9] Diaconis, P., Holmes, S. and Shahshahani, M. *Sampling from a manifold*, IMS Collections, **10**, 102–125, (2013).
- [10] Edelsbrunner, H., *A Short Course in Computational Geometry and Topology*, Springer, (2014).
- [11] Edelsbrunner, H. and Harer, J., *Persistent homology—a survey*, Contemp. Math., **453**, 257–282, (2008).
- [12] Edelsbrunner, H. and Harer, J.L., *Computational Topology, An introduction*, American Mathematical Society, Providence, RI, (2010).
- [13] Ghrist, R., *Elementary Applied Topology*, Createspace, (2014).
- [14] Oudot, S.Y., *Persistence Theory: From Quiver Representations to Data Analysis*, Mathematical Surveys and Monographs, **209**, (2015).
- [15] Robert, Christian P. and Casella, George. *Monte Carlo Statistical Methods*. Springer Texts in Statistics, Springer-Verlag, New York (2004).
- [16] Wasserman, L. *Topological data analysis*. arXiv 1609.08227 (2016).
- [17] Zomorodian, A.J., *Topology for Computing*, Cambridge Monographs on Applied and Computational Mathematics, **16**, (2005).

Sarit Agami

Andrew and Erna Viterbi Faculty of Electrical Engineering

Technion – Israel Institute of Technology

e-mail: sarit.agami@mail.huji.ac.il

Robert J. Adler
Andrew and Erna Viterbi Faculty of Electrical Engineering
Technion – Israel Institute of Technology
e-mail: radler@technion.ac.il